Scientific Research Publishing

Journal of Biosciences and Medicines, 2024, 12, 556-571
https://www.scirp.org/journal/jbm
ISSN Online: 2327-509X
ISSN Print: 2327-5081

Signs of Aneurysm Formation Learned from Rubber Balloon Inflation

Fumio Nogata[1*], Yasunari Yokota[2], Yoko Kawamura[2], Hiroyuki Morita[3], Yoshihiro Uno[4], William R. Walsh[5], Takahiko Kawamura[6], Nigishi Hotta[7,8], Kenji Kagechika[9]

[1]Gifu University, Gifu, Japan
[2]Faculty of Engineering, Gifu University, Gifu, Japan
[3]Department of General Medicine and General Internal Medicine, Gifu University School of Medicine, Gifu, Japan
[4]Department of General Medicine, Gifu Prefectural General Medical Center, Gifu, Japan
[5]Prince of Wales Hospital, University of New South Wales, Kensington, Australia
[6]Diabetes and Endocrine Internal Medicine, Chubu Rosai Hospital, Nagoya, Japan
[7]Nagoya University, Nagoya, Japan
[8]Chubu Rosai Hospital, Nagoya, Japan
[9]Anamizu General Hospital, Ishikawa, Japan
Email: *nognog2525@yahoo.co.jp, *ngfu2525@gmail.com

How to cite this paper: Nogata, F., Yokota, Y., Kawamura, Y., Morita, H., Uno, Y., Walsh, W.R., Kawamura, T., Hotta, N. and Kagechika, K. (2024) Signs of Aneurysm Formation Learned from Rubber Balloon Inflation. *Journal of Biosciences and Medicines*, **12**, 556-571.
https://doi.org/10.4236/jbm.2024.1211042

Received: September 29, 2024
Accepted: November 25, 2024
Published: November 28, 2024

Abstract

Aneurysms can be classified into two main types based on their shape: saccular (spherical) and fusiform (cylindrical). In order to clarify the formation of aneurysms, we analyzed and examined the relationship between external force (internal pressure) and deformation (diameter change) of a spherical model using the Neo-Hookean model, which can be used for hyperelastic materials and is similar to Hooke's law to predict the nonlinear stress-strain behavior of materials with large deformation. For a cylindrical model, we conducted an experiment using a rubber balloon. In the spherical model, the magnitude of the internal pressure Δp value is proportional to G (modulus of rigidity) and t (thickness), and inversely proportional to R (radius of the sphere). In addition, the maximum pressure Δp (max) is reached when λ (=expanded diameter/original diameter) is approximately 1.2, and the change in diameter becomes unstable (nonlinear change) thereafter. In the cylindrical model, localized expansion occurred at $\lambda = 1.32$ ($\lambda = 1.98$ when compared to the diameter at internal pressure $\Delta p = 0$) compared to the nearby uniform diameter, followed by a sudden rapid expansion (unstable expansion jump), forming a distinct bulge, and the radial and longitudinal deformations increased with increasing Δp, leading to the rupture of the balloon. Both models have a starting point where nonlinear deformation changes (rapid expansion) occur, so quantitative observation of the artery's shape and size is important to prevent aneurysm formation.

Keywords

Aneurysm Formation, Pressure-Inflation Characteristics, Elastic Instability, Expansion Signs, Saccular and Fusiform

1. Introduction

Aneurysms are balloon-like bulges in the walls of arteries and other blood vessels that are asymptomatic until they become significantly larger or rupture [1]. They occur in locally weakened part of the blood vessel wall, and the part that expands to more than 1.5 times the size of normal arterial diameter is called aneurysms [2]-[4]. Aneurysms can occur anywhere in the circulatory system, but are most common in the brain, thoracic aneurysms, abdominal aortic aneurysms (AAA) and legs [5]-[8]. Furthermore, because aneurysms can be fatal if they rupture, it is believed that it is very important to recognize the signs and prevent aneurysms before they occur.

On the other hand, Michael Faraday invented a rubber balloon in 1824 to conduct experiments on gas laws [9]. Since then, many studies have been reported on the mechanism of expansion and contraction of rubber balloons [10]-[14], their structure and deformation behavior, etc. These results (external forces and deformation characteristics) are very useful because rubber balloons resemble organs such as the heart, lungs, bladder, and arteries.

However, because the deformation behavior is complex, various theoretical models have been proposed [15]-[18]. Meanwhile, aneurysms can be classified into two main types based on their shape, saccular (spherical) and fusiform (cylindrical).

In this report, to clarify the formation of aneurysms, we analyzed and considered the relationship between the external force (internal pressure) and deformation (diameter change) for a spherical model using the Neo-Hookean model [17] [18], which can be used for hyperelastic materials and is similar to Hooke's law for predicting the nonlinear stress-strain behavior of materials with large deformation. For the cylindrical model, experiments were conducted using a rubber balloon. Both models have a starting point where nonlinear expansion deformation occurs with an increase in internal pressure, so we have shown the importance of detailed detection of gradual diameter changes that progress at both the macro- and micro-levels, especially changes just before a sudden increase in diameter.

2. Inflation of a Rubber Balloon: Pressure-Diameter Relation

2.1. Spherical Model

We consider from a mechanical perspective the expansion of a rubber balloon of original outer radius R and thickness t, as shown in **Figure 1**, using the Neo-Hookean which is a strain energy density function used to analyze hyperelastic

materials such as rubbers.

Suppose that the internal pressure (Δp) increases and the radius of the rubber wall of the spherical balloon increases λ time (the expansion ratio (d'o/do) of circumferences of the balloon in the inflated and uninflated states). Where do (=2R) is the outer diameter of the uninflated balloon, t'is the wall thickness after expansion, d'o is the outer diameter after expansion, σ_θ is circumferential stress, σ_z is stress in z direction, and σ_r is radial stress.

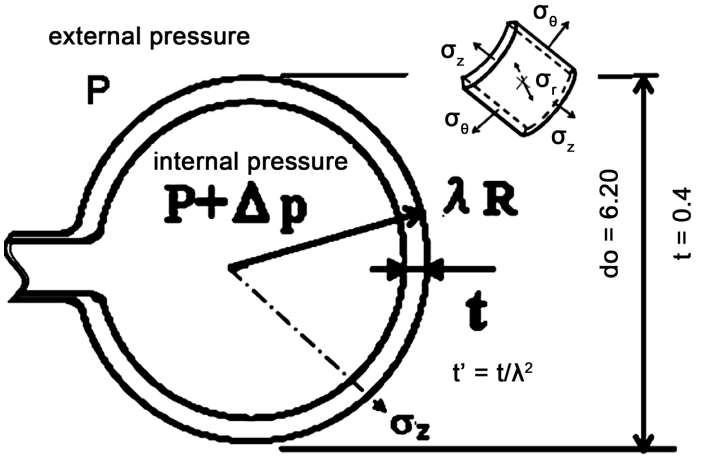

Figure 1. A spherical model of radius λR and thickness t subjected to internal pressure Δp.

Under incompressible and the volume is constant conditions, the wall thickness becomes t/λ^2, because the sphere deforms equally in three directions:

$$\lambda_i = \lambda_r \lambda_\theta \lambda_z = 1. \tag{1}$$

Therefore, from the elastic energy due to deformation of the rubber wall and the energy due to pressure change (Δp), the total free energy (E_{total}) can be calculated as follows [10].

$$E_{total} = 4\pi R^2 t (G/2)\left[2\lambda^2 + \left(1/\lambda^4\right) - 3\right] - \Delta P\left\langle 4\pi R^3 \left(\lambda^3 - 1\right)\right\rangle / 3. \tag{2}$$

where G is modulus of rigidity, λ (=d'o/do) is the ratio of the initial diameter (do) to expanded diameter (d'o), and the radius is R = do/2. The conditions for both to be in equilibrium are

$$\partial E_{total} / \partial \lambda = 0. \tag{3}$$

Therefore,

$$\Delta p = \frac{2tG}{R}\left[\left(1/\lambda\right) - \left(1/\lambda^7\right)\right] \tag{4}$$

This equation shows the relationship between Δp and balloon diameter, and also shows that beyond a certain threshold (maximum pressure Δp^*) there is no stable solution.

That is, depending on the mechanical properties of the material, it reaches the maximum value Δp^*, after which the diameter increases nonlinearly: a mechanical

instability that increases rapidly with diameter.

The magnitude of the value of internal pressure Δp is proportional to G and t, and inversely proportional to R. As an example, we considered the relationship between pressure and expansion.

Figure 2 shows the relationship between the internal pressure Δp and the expansion ratio λ (=di/do) for two different diameters (do = 2R) and t, where G = 0.24 kPa was used [19].

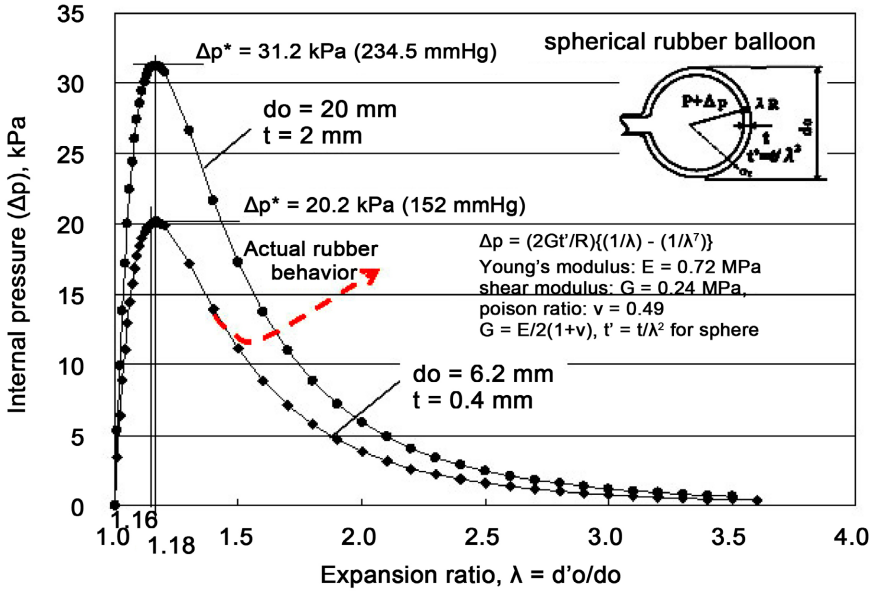

Figure 2. Pressure-expansion ratio (λ) characteristics of a spherical rubber balloon from the kinetic theory [10]. The rigidity modulus G value (0.24 GPa) was calculated from the authors' experimental data in the initial small deformation range (Appendix Figure A1, [19]).

The two curves were almost the same λ values at the Δp^* (λ = 1.16 and 1.18), even though their diameters and thicknesses differed by several times. For real rubber materials, simple forms of the kinetic theory of rubber, e.g. uniaxial force-extension curves, are limited in validity to approximately $\lambda < 3.5$, because at larger extensions crystallization occurs and the elasticity is no longer purely entropic ([20]: footnote, p. 23). For this reason, as an example, the red dashed line shows the actual behavior of rubber diagrammatically.

Based on the above mechanical knowledge, we reviewed the published risk data regarding aneurysm rupture by the report of the UCAS Japan [21].

The Japanese Society of Neurosurgery conducted an eight-year investigation into the rupture of unruptured cerebral aneurysms of 3 mm or larger discovered during examinations, with and without special treatment (natural observation) and with treatment. They investigated 6697 aneurysms (5720 patients) and presented the risk of rupture (%) in five size-based categories [22]. This report suggests that the size, location, and shape of the aneurysm are important risk factors, with larger sizes associated with higher rupture rates. Data compiled by the UCAS

Japan group regarding the size and rupture risk of cerebral aneurysms are shown in Graph 1(a), and changes in wall thickness and stress due to aneurysm expansion are shown in Graph 1(b): These wall stresses were calculated for the sizes in Graph 1(a) assuming a sphere under internal pressure. Details are given in the authors' report [23].

Figure 3 shows the relationship between pressure Δp and λ using Equation (2), assuming that the single sphere model with initial diameter do = 3 is extended to 25 mm, from the data in Graph 1(a) and Graph 1(b). This graph means that expansion deformation becomes mechanically unstable when the maximum pressure value Δp^{*} = 167 mmHg (22.2 kPa) or λ = 1.33 is exceeded as shown in the arrow whether or not the aneurysm ruptures will depend on the mechanical properties of the subject's arteries.

a) Aneurysm size and rupture risk classification according to the UCAS Japan report.

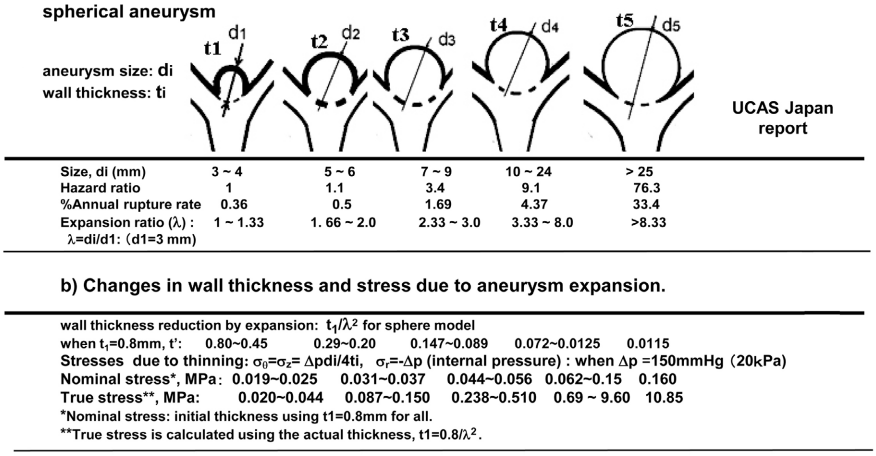

Size, di (mm)	3 ~ 4	5 ~ 6	7 ~ 9	10 ~ 24	> 25
Hazard ratio	1	1.1	3.4	9.1	76.3
%Annual rupture rate	0.36	0.5	1.69	4.37	33.4
Expansion ratio (λ) : λ=di/d1: (d1=3 mm)	1 ~ 1.33	1. 66 ~ 2.0	2.33 ~ 3.0	3.33 ~ 8.0	>8.33

b) Changes in wall thickness and stress due to aneurysm expansion.

wall thickness reduction by expansion: t_i/λ^2 for sphere model					
when t_1=0.8mm, t':	0.80~0.45	0.29~0.20	0.147~0.089	0.072~0.0125	0.0115
Stresses due to thinning: $\sigma_0=\sigma_z=\Delta pdi/4ti$, $\sigma_r=-\Delta p$ (internal pressure) : when Δp =150mmHg (20kPa)					
Nominal stress*, MPa:	0.019~0.025	0.031~0.037	0.044~0.056	0.062~0.15	0.160
True stress**, MPa:	0.020~0.044	0.087~0.150	0.238~0.510	0.69 ~ 9.60	10.85

*Nominal stress: initial thickness using t1=0.8mm for all.
**True stress is calculated using the actual thickness, $t1=0.8/\lambda^2$.

Graph 1. (a) Aneurysm size and rupture risk classification according to the UCAS Japan report [21] [22]; (b) Changes in wall thickness and wall stress for the sizes in (a), detailed calculations are given in the authors' report [23].

Figure 4 shows the increase in wall stress (nominal and true stress) from an initial aneurysm diameter of 3 mm to 25 mm, t = 0.8 mm (average thickness for adults, [24]) at internal pressures of 120 (16 kPa) and 150 mmHg (20 kPa).

Now let us compare these wall stresses to the strength of blood vessels. The authors previously performed uniaxial tensile and internal pressure tests on human common carotid artery specimens (CCA, 80-year-old) to obtain data on the strength ([25] [26], Appendix Figure A3). The results showed that the true stress was 0.37 to 2.38 MPa in tensile test, the elongation ratio at fractured λf = 1.40 to 2.18, and 0.86 to 1.70 MPa in internal pressure test, and the elongation ratio at ruptured λf = 1.20 to 1.87 (Appendix, Figure A4).

When these measurement data are matched with the wall stress curve in Figure 4, the range is λ = 3.5 to 5.6 (do = 10 to 17 mm), and AB within this range has a hazard ratio of 9.1 as specified by UCAS Japan, which is considered to have sufficient strength to accommodate aneurysm diameters up to approximately 17 mm.

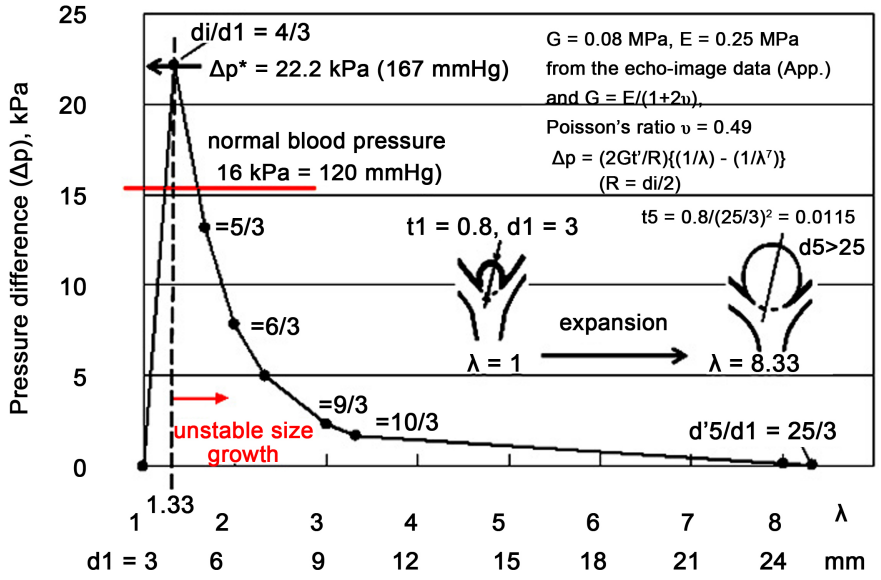

Figure 3. Pressure (Δp)—expansion ratio (λ) characteristic of human artery (the UCAS Japan data) according to the kinetic theory: when the λ value exceeds 1.33, the diameter increases unstably, as shown by the red arrow. The human stiffness modulus, G = 0.08 MPa (common carotid artery, CCA), was obtained from the authors' clinical data by echo-video analysis (Appendix Figure A2).

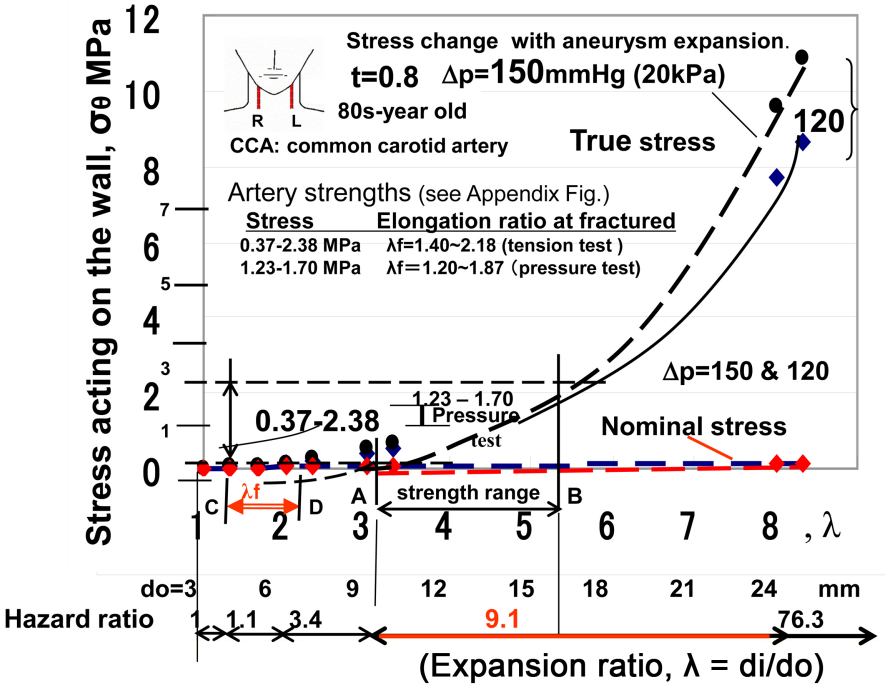

Figure 4. Wall stress and human arterial strength with increasing aneurysm size in the UCAS Japan model: AB is the range based on arterial strength, and CD is the range of elongation (in the 80s) at rupture. Note that even if strength is sufficient, reduced elongation (embrittlement) can significantly contribute to rupture.

On the other hand, the stress value λf (1.40 - 2.18: Appendix Figure A4) in the

CD range was very small, with a hazard ratio of 1.1 (d'o = 4 - 7 mm).

This means that the possibility of blood vessel rupture increases as the tensile deformation (brittleness) decreases. For reference, Appendix Figure A5 compares a young sheep's artery and a rubber balloon with a human artery. It is clear that the burst elongation of human arteries decreases with age. This may be one of the reasons why blood vessels burst without warning. Therefore, it is important to measure stiffness, strength, and tensile deformation of arteries from young adulthood.

2.2. Cylindrical Model

Assuming the shape of a fusiform aneurysm, an internal pressure load experiment was conducted using a cylindrical rubber balloon whose axial length was sufficiently longer than the wall thickness so that the mechanical effects due to the shape of both ends could be ignored.

Figure 5 shows the changes in the contour shape and dimensions of a rubber

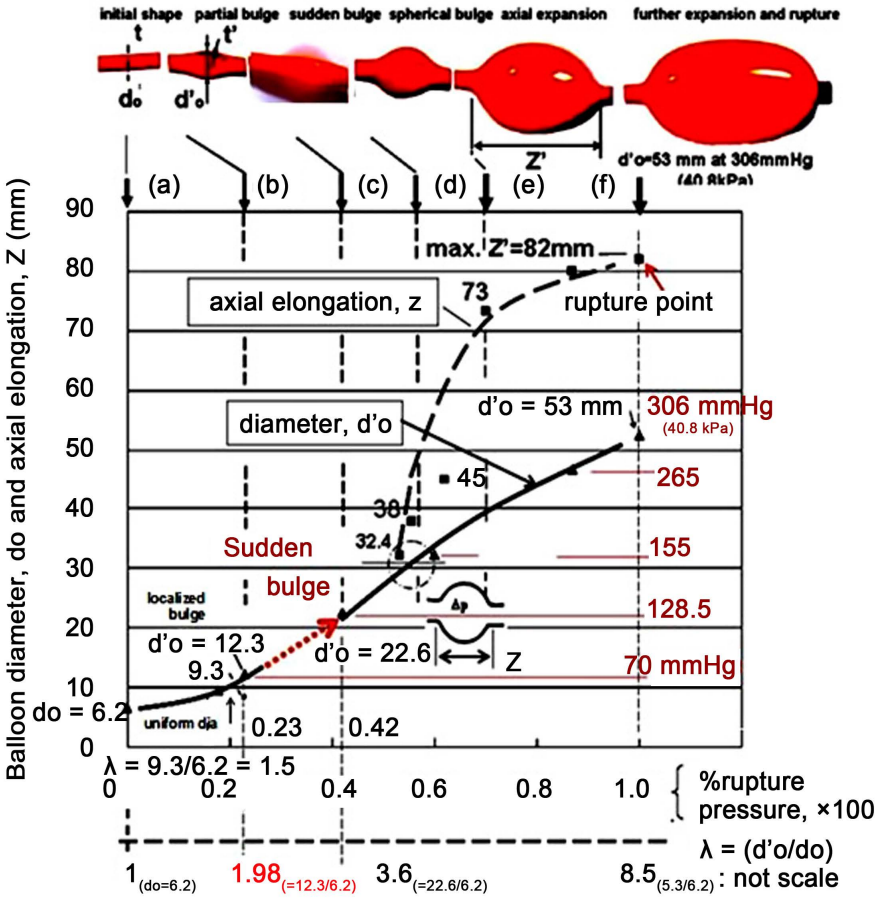

Figure 5. The change in contour and dimensions of a balloon until it ruptures. The true stress and the nominal stress at the rupture: Δp = 306 mmHg = 40.7 kPa, $t' = 1/(\lambda_\theta)$ = (0.4/8.55) = 0.046 mm, $\sigma_z = (\sigma_\theta/2)$, $\sigma_r = -\Delta p$ at the inner wall, $\sigma_r = -\Delta p = 0$ at the outer wall, nominal stress $\sigma_\theta = \sigma_\theta = \Delta pR/to$ = (40.7 × (53/2)/0.4)/1000 = 2.7 MPa, true stress $\sigma_\theta = pr/t'$ = (40.7 × (53/2)/0.046)/1000 = 23.4 MPa.

balloon (diameter do = 6.2 mm, thickness t = 0.2 mm) until it ruptures. From the equation for a thin-walled cylinder subjected to internal pressure Δp, the circumferential stress $\sigma_\theta = \Delta pR/t$, the axial stress $\sigma_z = \Delta pR/2t = \sigma_\theta/2$, the radial stress $\sigma_r = -\Delta pR/t$ on the inner wall, and $\sigma_r = 0$ on the outer wall. Therefore, σ_z is half the circumferential stress σ_θ. The photographs above show (a) the initial shape, (b) the expansion of diameter with increasing internal pressure and the appearance of small local bulges, (c) the sudden expansion of diameter with increasing internal pressure, followed by (d) nearly sphere, (e) expansion in diameter and length in the Z direction, and (f) just before it ruptures.

The characteristic change was that the pressure increased from Δp = 70 mmHg (9.3 kPa, 23% of the rupture pressure) and suddenly a large bulge formed at 128.5 mmHg (17 kPa), changing in diameter from do' = 12.3 mm (λ' = 1.98) to 22.6 mm (λ' = 22.6/6.2 = 3.6). Then, at about 155 mmHg (20.6 kPa), it became a sphere with a diameter of about 32 mm. Then, the elongation in the z direction increased and it rupture at a diameter of ϕ 53 mm, z = about 82 mm. These data show that, like the spherical model mentioned above, the cylindrical model also has a region of mechanical instability that increases rapidly with diameter.

Figure 6 shows a photograph of the moment when the bulge formed due to instability expansion jump. It was taken from a recorded video frame (1/30 s). From the left, we see the size of the original shape (ϕ 6.2 mm), uniform expansion at 70 mmHg (ϕ 9.3 mm), slight partial expansion of about d'o = ϕ 12.3 mm, and the instability jump at λ' = 2.43 at that point. Analysis by Muller *et al*. ([27], p: 38) reports that from kinetic theory [10], the onset of mechanical instability ΔP^* occurs at λ' = 1.7 or more.

Similar to the pressure-inflation ratio (λ = 1.18 in Figure 2) characteristic of the spherical rubber balloon mentioned above, even in the cylindrical shape, an increase in diameter can occur due to a sudden change in the instability expansion jump [28]-[30]. It is important to note that aneurysm formation does not begin as a slow swelling, but rather as slight partial expansion until mechanical instability occurs and then grows rapidly.

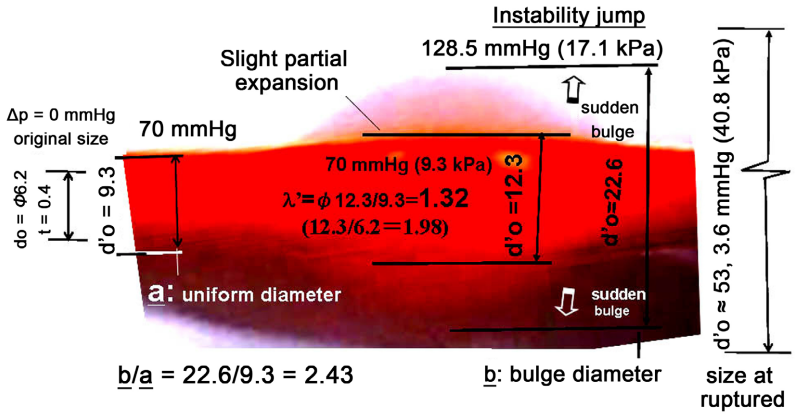

Figure 6. A photograph of the moment the bulge formed (from d'o = 9.3, and 12.3 to 22.6 mm in Figure 5). The largest bulge was generated at λ' = b/a = 22.6/9.3 = 2.43.

Figure 7 is a photograph shown in a study by Kugo *et al.* to the development of a drug to shrink aneurysms of human abdominal aortic aneurysms (AAA) [30]. From the figure, the ratio of the diameter of the uniform part ($\underline{a}$) to the aneurysm diameter ($\underline{b}$) was $\lambda = \underline{b}/\underline{a} = 2.1$.

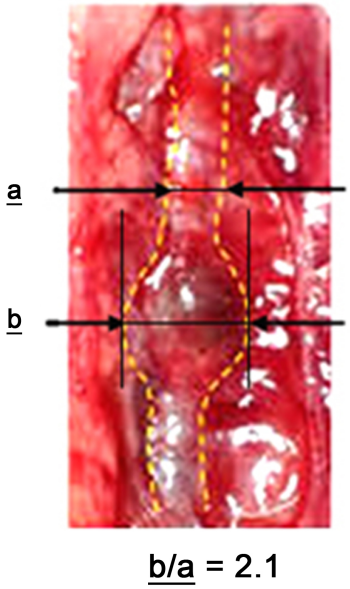

Figure 7. A Photograph shown in the research by Kugo *et al.* on the development of a drug to shrink aneurysms [31].

	Kinetic theory instability	Slight partial expanding	Aneurysm formation due to instability jump	Remarks
Spherical model				
Rubber balloon				
λ':	1.18 (Fig. 2)	-	[27]	-
Human artery				
λ':	1.33 (Fig. 3)	-		-
Cylindrical model				
Rubber balloon				
λ=d'o/do:	1.7 [27]	12.3/6.2 =1.98 (Fig.5, 6)	22.6 / 6.2=3.64 (Fig.5, 6)	do=6.2 at 0 mmHg*
λ =d'o/do:	-	12.3/ 9.3 =1.32	22.6 / 9.3=2.43 (Fig.5, 6)	do=9.3 at 70 mmHg*
Human artery:				
λ':	-	-	2.1 (Fig. 7)	

*1 mmHg=0.133kPa

Graph 2. Signs of aneurysm formation and its changes in shape.

In this paper, we discussed the mechanical behavior of rubber balloons and human arteries from the same perspective. Historically, this has been done by analogy with biological organs such as the heart, lungs, and bladder [10]-[14]. Here too, the emphasis has been on finding signs of aneurysm formation. One of the reasons for this is the similarity of the behavior of the stress-elongation λ graphs of human arteries, young sheep arteries, and rubber balloons in uniaxial tensile

tests, as shown in Figure A5 in the Appendix.

Graph 2 summarizes shape changes in the signs of aneurysm formation. The diameter ratio (λ) at the onset of aneurysm formation due to kinetic instability, partial slight expansion, and instability jump is shown. Although the data is limited, looking at these figures, it can be said that a slight bulge of about 1.3 times or more indicates the possibility of aneurysm formation. Therefore, to prevent the development of aneurysms, it is important to detect and monitor partial bulges of uniform diameter, and attention to these diameter ratios λ may be an indicator. Monitoring of blood pressure is also important.

3. Concluding Remarks

In order to clarify the process of aneurysm formation, the external force (internal pressure, Δp) versus deformation (diameter expansion) characteristics of a spherical model were analyzed and examined using the Neo-Hookean model. For a cylindrical model, experiments were conducted using a rubber balloon.

1) For the spherical model, the magnitude of the Δp value is proportional to G (modulus of rigidity) and t (thickness), and inversely proportional to R (radius of the sphere).

The internal pressure-deformation relationship according to the kinetic theory reaches the maximum pressure Δp (max) when λ (=expanded diameter/original diameter) is approximately 1.2 or more, and then the change in diameter becomes unstable (nonlinear change).

In other words, the diameter may expand significantly depending on the mechanical properties of the material.

2) For the cylindrical model, when a small local bulge exceeds λ (the ratio to the surrounding uniform diameter) of 1.32, it expands rapidly to form a distinct bulge, and as Δp increases, the diameter and longitudinal deformation increase, leading to the balloon bursting.

Both models have a starting point where nonlinear deformation changes (rapid expansion) occur, so if we can detect in detail the gradual partial diameter changes that progress globally and locally, especially the changes just before the diameter ratio λ increases suddenly, it may be possible to prevent the expansion of aneurysms.

Acknowledgements

The authors would like to express their gratitude to the undergraduate and graduate students who participated in related research in our laboratory from 2005 to 2012. The clinical studies were conducted in accordance with the regulations of the ethical committees of Gifu University Hospital and the hospital to which the co-authors are affiliated.

Conflicts of Interest

The authors declare no conflicts of interest regarding the publication of this paper.

References

[1] NIH Health Information, National Neurological Disorders and Stroke (2024) Cerebral Aneurysms. https://www.ninds.nih.gov/health-information/disorders/cerebral-aneurysms

[2] Hiroshima University, Graduate School of Biomedical & Sciences (Cardiovascular Surgery), Japan (2023) What's an Aneurysm? Q and A. https://surgery1.hiroshima-u.ac.jp/about/diagnosis/Cardiovascular/whats-an-aneurysm-q-and-a/

[3] Johnston, K.W., Rutherford, R.B., Tilson, M.D., Shah, D.M., Hollier, L. and Stanley, J.C. (1991) Suggested Standards for Reporting on Arterial Aneurysms. *Journal of Vascular Surgery*, **13**, 452-458. https://doi.org/10.1067/mva.1991.26737

[4] Chaikof, E.L., Brewster, D.C., Dalman, R.L., Makaroun, M.S., Illig, K.A., Sicard, G.A., *et al.* (2009) The Care of Patients with an Abdominal Aortic Aneurysm: The Society for Vascular Surgery Practice Guidelines. *Journal of Vascular Surgery*, **50**, S2-S49. https://doi.org/10.1016/j.jvs.2009.07.002

[5] Patel, M.I., Hardman, D.T., Fisher, C.M. and Appleberg, M. (1995) Current Views on the Pathogenesis of Abdominal Aortic Aneurysms. *Journal of the American College of Surgeons*, **181**, 371-382.

[6] Sakalihasan, N., Limet, R. and Defawe, O. (2005) Abdominal aortic aneurysm. *The Lancet*, **365**, 1577-1589. https://doi.org/10.1016/s0140-6736(05)66459-8

[7] Thompson, B.G., Brown, R.D., Amin-Hanjani, S., Broderick, J.P., Cockroft, K.M., Connolly, E.S., *et al.* (2015) Guidelines for the Management of Patients with Unruptured Intracranial Aneurysms. *Stroke*, **46**, 2368-2400. https://doi.org/10.1161/str.0000000000000070

[8] Juvela, S., Porras, M. and Heiskanen, O. (1993) Natural History of Unruptured Intracranial Aneurysms: A Long-Term Follow-Up Study. *Journal of Neurosurgery*, **79**, 174-182. https://doi.org/10.3171/jns.1993.79.2.0174

[9] Eye Up Events (2023) The History of Balloon Twisting. https://www.eyesup.events/blog/the-history-of-balloon-twisting

[10] Muller, I. and Strehlow, P. (2004) Rubber and Rubber Balloons: Paradigms of Thermodynamics. In *Lecture Notes in Physics* (Volume 637), 21-34.

[11] Ajmal, A., *et al.* (2023) Properties of Rubber Balloons: Addtitional Notes. https://physlab.org/wp-content/uploads/2023/01/student_manual_additional_notes.pdf

[12] Atkins, J.E. and Rivlin, R.S. (1951) Large Elastic Deformations of Isotropic Materials IX. The Deformation of Thin Shells. Davy Faraday Laboratory of the Royal Institution.

[13] Mooney, M. (1940) A Theory of Large Elastic Deformation. *Journal of Applied Physics*, **11**, 582-592. https://doi.org/10.1063/1.1712836

[14] Rivlin, R.S. (1948) Large Elastic Deformations Isotropic Materials. IV. Further Developments of the General Theory. *Philosophical Transactions of the Royal Society A*, **241**, 379-397.

[15] Müller, I. and Struchtrup, H. (2002) Inflating a Rubber Balloon. *Mathematics and Mechanics of Solids*, **7**, 569-577. https://doi.org/10.1177/108128650200700506

[16] Dreyer, W., Müller, I. and Strehlow, P. (1982) A Study of Equilibria of Interconnected Balloons. *The Quarterly Journal of Mechanics and Applied Mathematics*, **35**, 419-440. https://doi.org/10.1093/qjmam/35.3.419

[17] WELSIM (2021) Neo-Hookean Hyperelastic Model for Nonlinear Finite Element Analysis. https://welsim.com/2021/04/17/neo-hookean-hyperelastic-model-for-nonlinear-finite-element-analysis.html

[18] Bucchi, A. and Hearn, G.E. (2013) Predictions of Aneurysm Formation in Distensible Tubes: Part A—Theoretical Background to Alternative Approaches. *International Journal of Mechanical Sciences*, **71**, 1-20. https://doi.org/10.1016/j.ijmecsci.2013.02.005

[19] Nogata, F., Yokota, Y., Kawamura, Y., Mouri, T., Walsh, W.R., Kawamura, T. and Hotta, N. (2019) Towards the Application of AI Technology to Assess Risk of Aneurysm Rupture Based on Medical Imaging: Relations of Geometry, Size, Blood Pressure, and Wall Strength. *International Journal of Computing & Information Technology*, **8**, 120-130. https://www.researchgate.net/profile/Fumio-Nogata/research

[20] Muller, I. and Strehlow, P. (2004) Rubber and Rubber Balloons: Paradigms of Thermodynamics. Springer. https://doi.org/10.1007/b93853

[21] Morita A., *et al*. (2012) The Natural Course of Unruptured Cerebral Aneurysms in a Japanese Cohort. *New England Journal of Medicine*, **366**, 2474-2482. https://doi.org/10.1056/nejmoa1113260

[22] Guidelines for Diagnosis and Treatment of Aortic Aneurysm and Aortic Dissection (2011) The Digest Version by JCS Joint Working Group by Japanese Circulation Society and Other Six Societies. (In Japanese) http://jns.umin.ac.jp/member/UCAS/ucas.html

[23] Nogata, F., Yokota, Y., Kawamura, Y., Morita, H., Uno, Y., Mouri, T., *et al.* (2021) Biomechanical Considerations in the Unruptured Cerebral Aneurysm Study (UCAS Japan): Rupture Risk and True Stress of Wall. *Journal of Biosciences and Medicines*, **9**, 172-189. https://doi.org/10.4236/jbm.2021.910015

[24] Park, E. (1978) Age-Related Change of the Wall of Arteries in Human Adults. *Journal of the Showa Medical Association*, **38**, 581-592. https://doi.org/10.14930/jsma1939.38.581

[25] Nogata, F., Yokota, Y., Kawamura, Y., Walsh, W.R., Morita, H., Uno, Y., *et al.* (2009) A Technique for Estimating Sclerosis of Carotid Artery with Ultrasonic Echo. *IFMBE Proceedings*, **25**, 655-658. https://doi.org/10.1007/978-3-642-03882-2_175

[26] Nogata, F., Yokota, Y., Kawamura, Y., Morita, H. and Uno, Y. (2007) Estimating of Mechanical Strength of *in Vivo* Common Carotid Artery Using Ultrasound Echo Images. *Proceedings of ISBPE*/*The* 22*nd SICE Symposium*, Harbin, 249-252.

[27] Muller, I. and Strehlow, P. (2004) Rubber and Rubber Balloons: Paradigms of Thermodynamics. In *Lecture Notes in Physics* (Volume 637), 38.

[28] Anssari-Benam, A., Bucchi, A. and Saccomandi, G. (2021) Modelling the Inflation and Elastic Instabilities of Rubber-Like Spherical and Cylindrical Shells Using a New Generalised Neo-Hookean Strain Energy Function. *Journal of Elasticity*, **151**, 15-45. https://doi.org/10.1007/s10659-021-09823-x

[29] Anssari-Benam, A. and Bucchi, A. (2021) A Generalised Neo-Hookean Strain Energy Function for Application to the Finite Deformation of Elastomers. *International Journal of Non-Linear Mechanics*, **128**, Article ID: 103626. https://doi.org/10.1016/j.ijnonlinmec.2020.103626

[30] Zamani, V. and Pence, T.J. (2017) Swelling, Inflation, and a Swelling-Burst Instability in Hyperelastic Spherical Shells. *International Journal of Solids and Structures*, **125**, 134-149. https://doi.org/10.1016/j.ijsolstr.2017.07.010

[31] Kugo, H., Sugiura, Y., Fujishima, R., Jo, S., Mishima, H., Sugamoto, E., *et al.* (2023) Tricaprin Can Prevent the Development of AAA by Attenuating Aortic Degeneration. *Biomedicine & Pharmacotherapy*, **160**, Article ID: 114299. https://doi.org/10.1016/j.biopha.2023.114299

Appendix

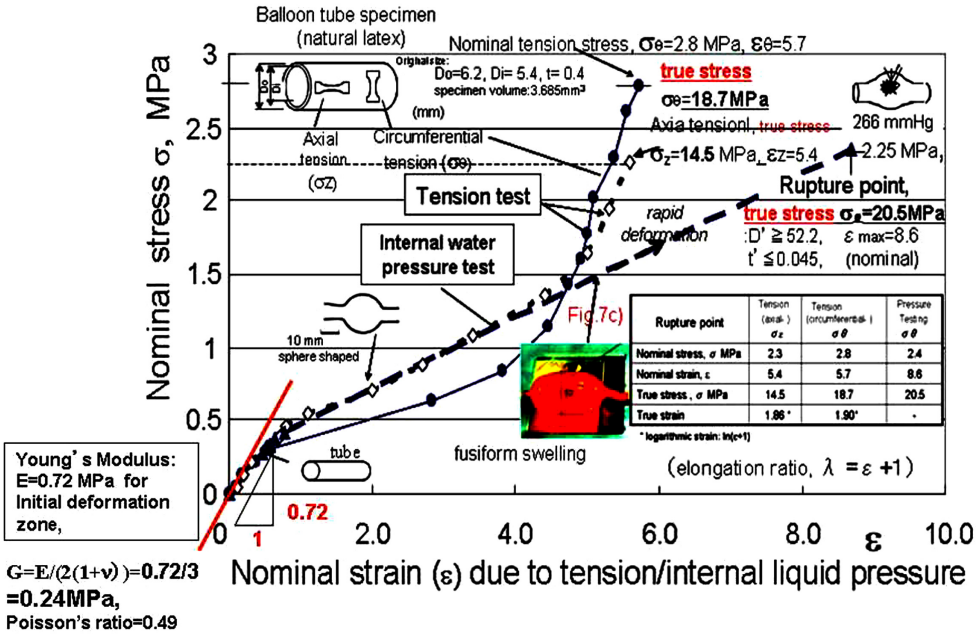

Figure A1. Nominal strain-stress curves of a rubber balloon: Young's modulus E = 0.72 GPa and rigidity modulus G = 0.24 GPa were obtained in the small deformation range.

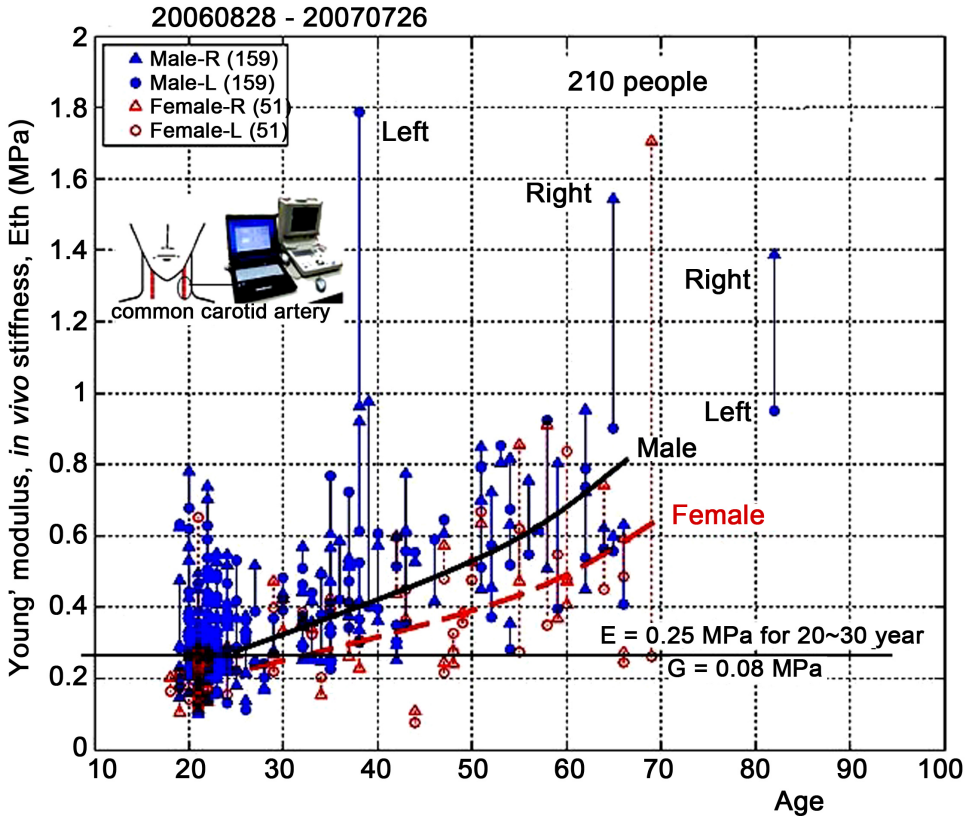

Figure A2. *In vivo* strength estimation data using B-mode ultrasound images from our laboratory. Data of E = 0.23 MPa, G = 0.24 GPa (20 - 30 years) were used for the discussion.

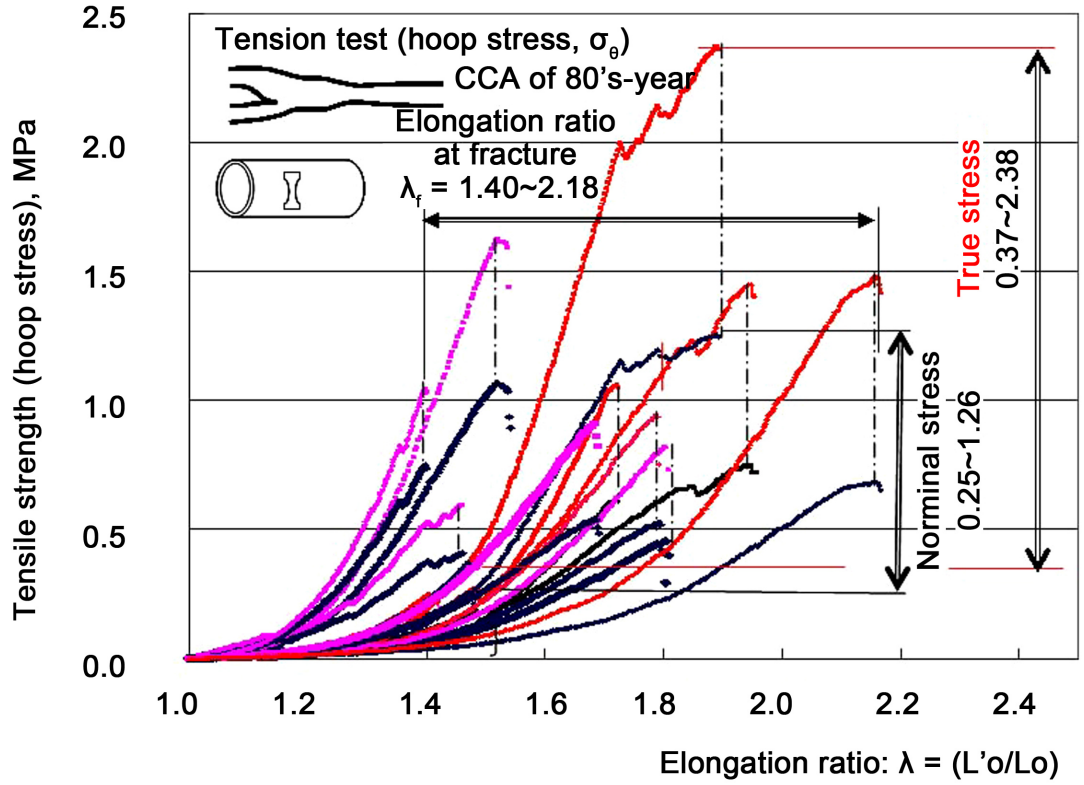

Figure A3. Tensile strength (true stress) range of the common carotid artery (CCA) in the 80s: it is clear that there is a large degree of individual variation.

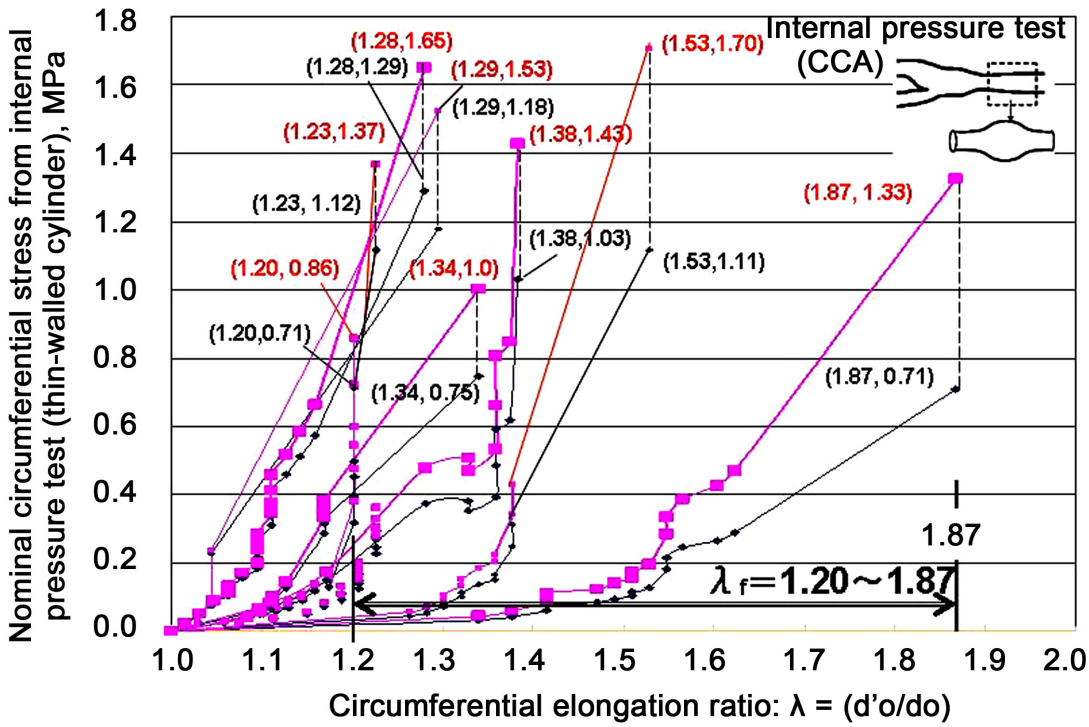

Figure A4. Tensile elongation range at break of common carotid artery (CCA) in the 80s. The red line shows true stress and black is nominal stress.

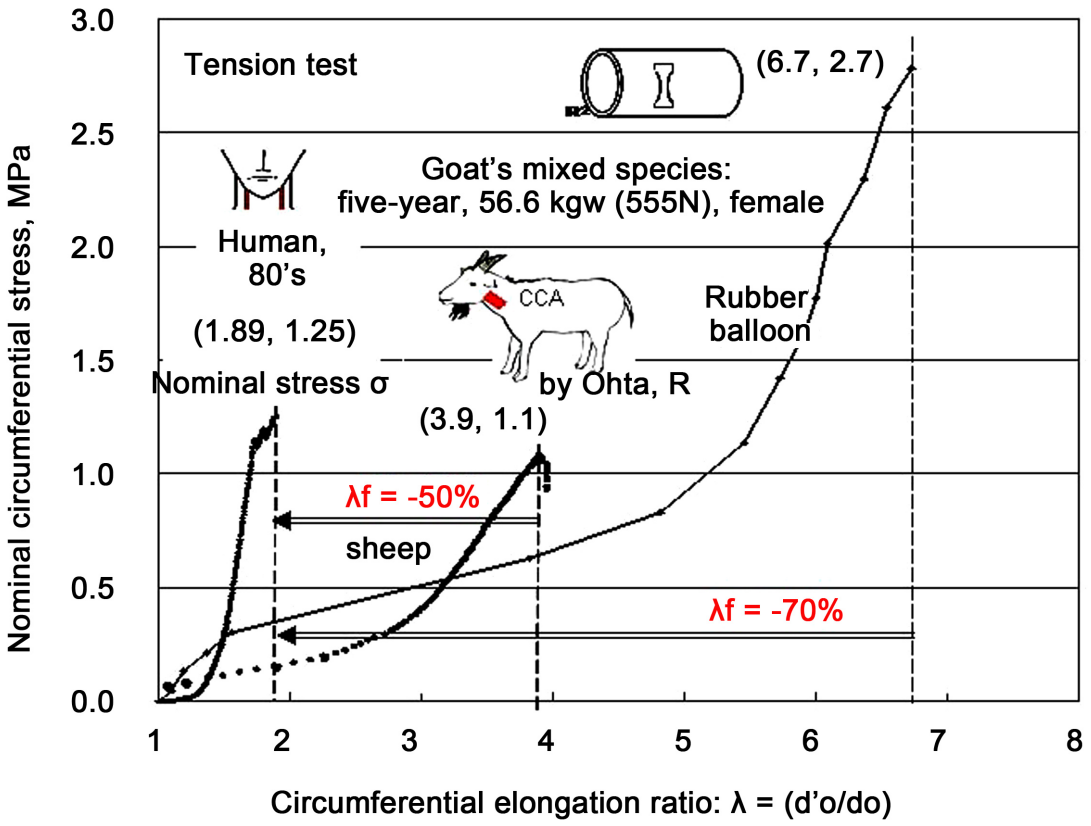

Figure A5. Comparison of the circumferential tensile elongation (λf) at ruptured for humans, sheep, and balloons: the curves showing the elastic to elastoplastic region show similar changes. The arteries of 80's are about 50% of the arteries of young sheep and about 30% of the arteries of balloons, showing significant stretch stiffening (arteriosclerosis). This is one of the reasons why balloons are used in mechanical property analysis studies of biological organs such as the heart, lungs, and bladder [10]-[14].